FOUNDATIONS
ADVANCES

ISSN: 2053-2733
journals.iucr.org/a

Indexing neutron transmission spectra of a rotating crystal

Adam Morawiec

Acta Cryst. (2024). A**80**, 379–386

Acta Cryst A FOUNDATIONS ADVANCES

ISSN 2053-2733

Indexing neutron transmission spectra of a rotating crystal

Adam Morawiec*

Institute of Metallurgy and Materials Science, Polish Academy of Sciences, Kraków, Poland. *Correspondence e-mail: nmmorawi@cyf-kr.edu.pl

Received 6 March 2024
Accepted 22 July 2024

Edited by L. Palatinus, Czech Academy of Sciences, Czechia

Keywords: neutron diffraction; neutron transmission spectra; Bragg dips; indexing; orientation determination.

Neutron time-of-flight transmission spectra of mosaic crystals contain Bragg dips, *i.e.*, minima at wavelengths corresponding to diffraction reflections. The positions of the dips are used for investigating crystal lattices. By rotating the sample around a fixed axis and recording a spectrum at each rotation step, the intensity of the transmitted beam is obtained as a function of the rotation angle and wavelength. The questions addressed in this article concern the determination of lattice parameters and orientations of centrosymmetric crystals from such data. It is shown that if the axis of sample rotation is inclined to the beam direction, the reflection positions unambiguously determine reciprocal-lattice vectors, which is not the case when the axis is perpendicular to the beam. Having a set of such vectors, one can compute the crystal orientation or lattice parameters using existing indexing software. The considerations are applicable to arbitrary Laue symmetry. The work contributes to the automation of the analysis of diffraction data obtained in the neutron imaging mode.

1. Introduction

Neutron studies of crystalline materials rely mainly on scattering methods, but neutron imaging can also be useful in research on such materials. In simple terms, neutron imaging involves measuring the attenuation of the transmitted beam, usually by radiography or tomography (Anderson *et al.*, 2009). Of interest here is wavelength-resolved imaging (Santisteban *et al.*, 2001; Woracek *et al.*, 2018). Neutron spectra recorded in transmission imaging geometry using the time-of-flight technique carry information about the crystal structure. The intensity of the transmitted beam is affected by crystal diffraction, and analysis of the recorded intensities allows conclusions to be drawn about the geometry of the crystal lattice. With this approach, crystallographic information is extracted from diffraction effects observed using a single wavelength-resolving point detector, and data are collected on imaging beamlines. The spatial resolution of wavelength-resolved transmission imaging is significantly better than that of conventional neutron diffraction (Woracek *et al.*, 2018).

Neutron transmission spectra of mosaic crystals contain minima (known as Bragg dips) at locations corresponding to diffraction reflections (Halpern *et al.*, 1941; Frikkee, 1975; Thiyagarajan *et al.*, 1998; Santisteban, 2005). The positions and shapes of the dips depend on the material, the orientation and the degree of perfection of the crystal. They can be used to determine the beam direction in the crystal reference frame and to study crystal orientation, mosaicity, lattice parameters or elastic strain (Malamud & Santisteban, 2016). Individual 'Bragg-dip patterns' have been used for 'orientation' and strain mappings (Sato *et al.*, 2017, 2018; Strickland *et al.*, 2020; Watanabe *et al.*, 2020; Sakurai *et al.*, 2021; Shishido *et al.*, 2023;

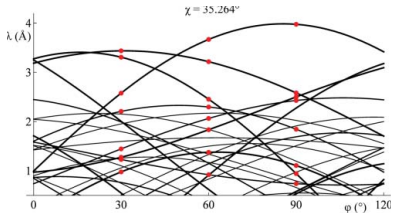

Watanabe *et al.*, 2024). However, the crystallographic information contained in a single spectrum is insufficient to fully characterize the crystal orientation or strain. The information is richer when multiple spectra are collected at various sample orientations. The simplest way to vary these orientations is to rotate the sample around a fixed axis in equiangular steps. By recording a spectrum at each rotation step, one obtains the intensity of the transmitted beam as a function of the rotation angle φ and the wavelength λ (Cereser *et al.*, 2017; Dessieux *et al.*, 2023*a*,*b*). The function can be seen as a diffraction pattern in (φ, λ) coordinates.

Combining wavelength-resolved imaging with detection of diffraction spots enabled Cereser *et al.* (2017) to map orientations of a multigrain sample in three dimensions. That mapping required a fully automatic procedure. It was based on forward 'indexing', *i.e.*, orientations were determined by comparing experimental patterns with patterns simulated for all possible orientations. Forward 'indexing' avoids the use of a 'backward' relationship leading from the pattern geometry to the crystal orientation. However, there are advantages to knowing and understanding this relationship. It can be used to search for experimental configurations favorable for determination of the lattice or its orientation.

The questions addressed here concern characterization of the crystal lattice using an experimental setup in which the sample rotation axis is not necessarily perpendicular to the beam direction. Having multiple spectra collected from a centrosymmetric crystal rotated about a fixed axis, what are the algorithms for determining crystal orientations or methods for estimating lattice parameters? Closely related are the issues of uniqueness of the resulting orientations and parameters.

It is shown below that if the axis of sample rotation is inclined to the beam direction, reciprocal-lattice vectors can be unambiguously determined from the positions of Bragg dips in neutron transmission spectra. (There is an ambiguity in the determination of these vectors when the axis is perpendicular or parallel to the beam.) Knowledge of several vectors of a lattice is the foundation for its full characterization. Schemes for both orientation determination and *ab initio* indexing are described. They are based on existing software. The methods presented are applicable to arbitrary Laue symmetry.

Throughout the article, vectors are identified with one-column matrices. Unit vectors are denoted by the 'hat' symbol $\hat{}$. Rotation by the angle α about axis parallel to the vector $\hat{\mathbf{n}}$ will be denoted by $R(\hat{\mathbf{n}}, \alpha)$. The same symbol will be used for the 3×3 special orthogonal matrix representing the rotation. The matrix is defined in such a way that the result of its operation on vector $\mathbf{v}$ is $R(\hat{\mathbf{n}}, \alpha)\mathbf{v} = \cos\alpha\,\mathbf{v} + (1 - \cos\alpha)(\hat{\mathbf{n}} \cdot \mathbf{v})\,\hat{\mathbf{n}} + \sin\alpha\,\mathbf{v} \times \hat{\mathbf{n}}$.

2. Pattern of sinusoidal curves

A Bragg dip in the spectrum is the result of crystal diffraction. First, one needs to link the wavelength at which the dip occurs with the reciprocal-lattice node corresponding to the dip. Let $\mathbf{k}_0$ and $\mathbf{k}$ be the wavevectors of the incident and diffracted beams, respectively. The geometry of crystal diffraction is described by the energy conservation law $|\mathbf{k}| = 1/\lambda = |\mathbf{k}_0|$ and the property that the scattering vector $\mathbf{k} - \mathbf{k}_0$ points to a node of the crystal reciprocal lattice. Analysis of crystal diffraction data involves three right-handed Cartesian reference systems: the one associated with the laboratory (indicated by the superscript L), the sample reference system (S) and the system attached to the crystal (C). Vectors with components in different reference frames will be denoted by different symbols. Let $\mathbf{g}^{\mathrm{L}}$ be the array with components of a reciprocal-lattice vector in the laboratory reference frame. With the wavevectors given in the same reference frame, based on $\mathbf{k} - \mathbf{k}_0 = \mathbf{g}^{\mathrm{L}}$, one has $(\mathbf{k} + \mathbf{k}_0) \cdot \mathbf{g}^{\mathrm{L}} = \mathbf{k}^2 - \mathbf{k}_0^2 = 0$, and elimination of $\mathbf{k}$ leads to

$$\mathbf{g}^{\mathrm{L}} \cdot (\mathbf{g}^{\mathrm{L}} + 2\mathbf{k}_0) = 0. \tag{1}$$

Let the reciprocal-lattice vector in the Cartesian reference frame attached to the crystal be denoted by $\mathbf{h}$.[1] With O standing for the special orthogonal matrix representing crystal orientation in the sample reference frame [Bunge's convention (Bunge, 1982; Morawiec, 2004)], the array $\mathbf{g} = O^T\mathbf{h}$ has components in the sample reference frame and is related to $\mathbf{g}^{\mathrm{L}}$ via

$$\mathbf{g}^{\mathrm{L}} = R_\varphi \mathbf{g}, \tag{2}$$

where R_φ is the special orthogonal matrix representing the (φ-dependent) orientation of the sample reference frame with respect to the laboratory reference frame. Substitution of $\mathbf{g}^{\mathrm{L}}$ given by (2) into (1) leads to

$$\mathbf{h}^2 + 2(R_\varphi O^T\mathbf{h}) \cdot \mathbf{k}_0 = 0, \tag{3}$$

where $\mathbf{h}^2$ is an abbreviation for $\mathbf{h} \cdot \mathbf{h}$. With $\hat{\mathbf{k}}_0 = \lambda\mathbf{k}_0$, one has $\lambda(\varphi) = -(2/\mathbf{h}^2)(O^T\mathbf{h}) \cdot (R_\varphi^T\hat{\mathbf{k}}_0)$, or briefly

$$\lambda(\varphi) = \hat{\mathbf{k}}^{\mathrm{S}}(\varphi) \cdot \mathbf{d}, \tag{4}$$

where $\hat{\mathbf{k}}^{\mathrm{S}}(\varphi) = R_\varphi^T\hat{\mathbf{k}}_0$ and $\mathbf{d} = -(2/\mathbf{h}^2)O^T\mathbf{h} = -(2/\mathbf{g}^2)\mathbf{g}$. The wavelength λ as a function of φ is a sinusoid of period 2π. Only parts of the sinusoid with $\lambda(\varphi) > 0$ are physically meaningful. Since multiple reflecting planes (and corresponding vectors $\mathbf{h}$) are involved, multiple sinusoidal curves appear in a pattern. Example patterns of sinusoids in (φ, λ) coordinates are shown in Fig. 1.

Knowing $\mathbf{d}$, one can calculate the corresponding reciprocal-lattice vector in the sample reference frame,

$$\mathbf{g} = -(2/\mathbf{d}^2)\,\mathbf{d}. \tag{5}$$

Therefore, the prior step is to determine the sinusoid parameters $\mathbf{d}$ from $\lambda(\varphi)$ and $\hat{\mathbf{k}}^{\mathrm{S}}(\varphi)$ using equation (4).

[1] For notational consistency, this vector could be denoted as $\mathbf{g}^{\mathrm{C}}$, but the symbol $\mathbf{h}$ is preferred in order to have the same notation as in related papers referred to below. The same applies to $\mathbf{g} = \mathbf{g}^{\mathrm{S}}$.

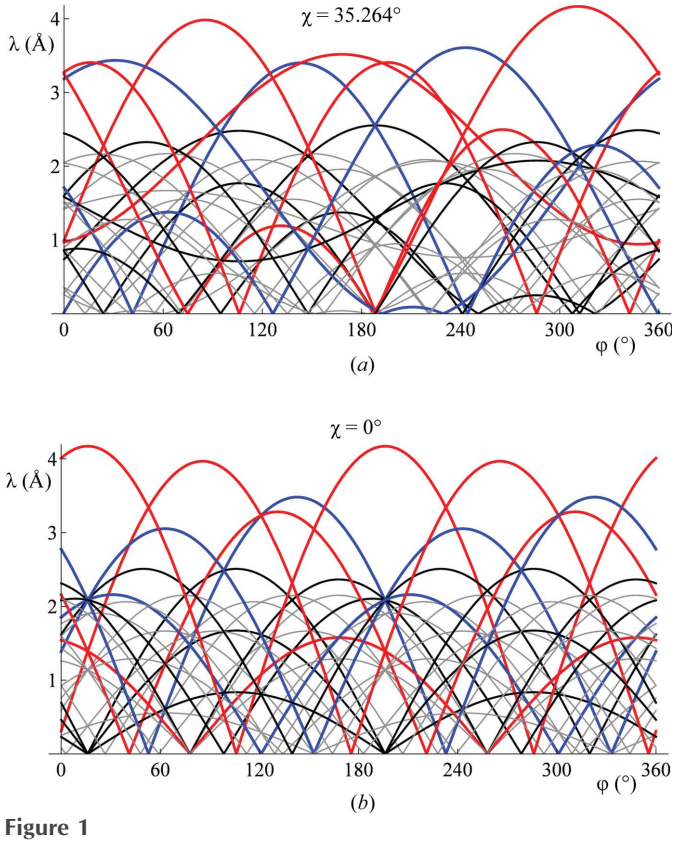

Figure 1
Simulated patterns of sinusoidal curves for a Cu crystal with the plane (1 2 3) perpendicular to the sample rotation axis $\mathbf{e}_3^{\mathrm{S}}$ and the crystal direction $[\bar{6}\,\bar{3}\,4]$ along sample's $\mathbf{e}_1^{\mathrm{S}}$ direction. (The orientation can be seen as a variant of the orientation *S* common in textures of face-centered-cubic metals.) The lattice parameter a = 3.61334 Å was used. Families of reflecting planes are {111} (red), {200} (blue), {220} (black), {311} (gray). The angle χ between the plane perpendicular to the incident beam and the axis of specimen rotation is 35.264° in (*a*) and 0° in (*b*). Periods of the patterns in (*a*) and (*b*) are 360° and 180°, respectively.

3. Parameters of sinusoids

Without losing generality, one can assume that the basis vector $\mathbf{e}_1^{\mathrm{L}}$ of the laboratory reference frame is along $\mathbf{k}_0$, $\mathbf{e}_3^{\mathrm{S}}$ is along the axis of crystal rotation and lies in the plane spanned by $\mathbf{k}_0$ and $\mathbf{e}_3^{\mathrm{L}}$, and the scalar products $\mathbf{k}_0 \cdot \mathbf{e}_1^{\mathrm{L}}$, $\mathbf{k}_0 \cdot \mathbf{e}_3^{\mathrm{S}}$ and $\mathbf{e}_3^{\mathrm{L}} \cdot \mathbf{e}_3^{\mathrm{S}}$ are non-negative (Fig. 2). With these assumptions and fixed $\chi = \arccos(\mathbf{e}_3^{\mathrm{L}} \cdot \mathbf{e}_3^{\mathrm{S}})$, one has $\hat{\mathbf{k}}_0 = [1\ 0\ 0]^T$, $0 \le \chi \le \pi/2$, $R_\varphi = R(\mathbf{e}_2^{\mathrm{L}}, \chi)^T R(\mathbf{e}_3^{\mathrm{S}}, \varphi)$ and $\hat{\mathbf{k}}^{\mathrm{S}}(\varphi) = [\cos\chi\cos\varphi \quad \cos\chi\sin\varphi \quad \sin\chi]^T$.

Knowing wavelengths on a sinusoid at three different angles φ_j (j = 1, 2, 3 and $0 \le \varphi_j < 2\pi$), one has a system of three linear equations

$$\lambda(\varphi_j) = \hat{\mathbf{k}}^{\mathrm{S}}(\varphi_j) \cdot \mathbf{d} \tag{6}$$

for components of **d**. The coefficient matrix is the transpose of $K_{\mathrm{S}} = [\hat{\mathbf{k}}^{\mathrm{S}}(\varphi_1)\ \hat{\mathbf{k}}^{\mathrm{S}}(\varphi_2)\ \hat{\mathbf{k}}^{\mathrm{S}}(\varphi_3)]$. Its determinant is given by

$$\det(K_{\mathrm{S}}) = \sin\chi\cos^2\chi\,(\sin(\varphi_1 - \varphi_3) + \sin(\varphi_2 - \varphi_1) + \sin(\varphi_3 - \varphi_2)). \tag{7}$$

The determinant equals zero when χ equals 0 or $\pi/2$. Clearly, there is an essential difference between singular and non-singular cases; if the matrix K_{S} is singular, **d** is not unique, and this affects the determinability of the reciprocal-lattice vector **g**.

3.1. Singular cases

3.1.1. The case of $\chi = \pi/2$. The physical reason for the singularity at $\chi = \pi/2$ is obvious: rotation of the sample about an axis parallel to the beam does not affect the angles between reflecting planes and the beam. In this case, the sinusoids become straight lines, and since $\hat{\mathbf{k}}^{\mathrm{S}}(\varphi) = [0\ 0\ 1]^T$, the wavelength is determined by the third component of **d**. Clearly, spectra recorded during sample rotation contain the same information as a single spectrum. Indexing an individual spectrum is equivalent to determination of the transmitted beam direction in the crystal reference frame. This subject is addressed in Appendix A. It is easy to see that the orientations $OR(\mathbf{e}_3^{\mathrm{S}}, \xi)$ lead to the same pattern regardless of the angle ξ. Moreover, the same pattern is obtained after the sample is half-turned about an axis perpendicular to the beam. Thus, also the orientations $OR(\mathbf{e}_1^{\mathrm{S}}, \pi)R(\mathbf{e}_3^{\mathrm{S}}, \xi)$ lead to the same pattern as that for *O*.

3.1.2. The case of $\chi = 0$. The reason for the singularity at χ = 0 is more subtle: with varying φ, the impact of the change in the angle between the beam and the reflecting plane on the last component of **d** is canceled out by the change in the wavelength contributing to the pattern. Since $\hat{\mathbf{k}}^{\mathrm{S}}(\varphi) = [\cos\varphi\ \sin\varphi\ 0]^T$, the third component of **d** does not affect the sinusoid $\lambda(\varphi)$.

With χ = 0, the pattern of sinusoids has the period of π along φ, *i.e.*, the spectra at φ and $\varphi + \pi$ are identical: since $\mathbf{h}^2 = (-\mathbf{h})^2$ and $(R_\varphi O^T\mathbf{h}) \cdot \mathbf{k}_0 = (-O^T\mathbf{h}) \cdot (-R_\varphi^T\mathbf{k}_0) = (O^T(-\mathbf{h})) \cdot (R_{\varphi+\pi}^T\mathbf{k}_0) = (R_{\varphi+\pi}O^T(-\mathbf{h})) \cdot \mathbf{k}_0$, if equation (3) is satisfied, so is the relationship $(-\mathbf{h})^2 + 2(R_{\varphi+\pi}O^T(-\mathbf{h})) \cdot \mathbf{k}_0 = 0$. Thus, if there is a dip at (φ, λ) due to **h**, then there is a dip at $(\varphi + \pi, \lambda)$ due to $-\mathbf{h}$. The fact that the pattern of sinusoids has the period of π affects orientation determination. Let *C* denote the half-turn about $\mathbf{e}_3^{\mathrm{S}}$, *i.e.*, $C = R(\mathbf{e}_3^{\mathrm{S}}, \pi) = R_\pi$. Since $R_{\varphi+\pi}O^T = R_\varphi CO^T = R_\varphi(OC)^T$, the periodicity implies that the patterns for *O* and *OC* are identical.[2] This means that with χ = 0, there is an ambiguity in determining crystal orientation: two equally correct orientations *O* and *OC* result from each pattern. A scheme for determining the orientations *O* and *OC* based on data obtained with the crystal rotation axis perpendicular to the beam direction is sketched at the end of Appendix A.

Summarizing, the usual measurement geometry (see, *e.g.*, Santisteban, 2005; Malamud & Santisteban, 2016; Cereser *et al.*, 2017; Dessieux *et al.*, 2023*a*) with χ = 0 is not optimal for lattice characterization. There are non-equivalent crystal

[2] The problem of orientation ambiguity is mentioned in Cereser *et al.* (2017) and it is extensively addressed in the supplementary information to that paper. It is claimed that the orientations *O* (which equals U^T in the notation of Cereser *et al.*, 2017) and *COC* lead to the same pattern. Generally, this claim is false, *i.e.*, patterns from crystals at orientations *O* and *COC* are different. In the case of cubic crystals with the Cartesian axes along the fourfold symmetry axes, the presence of *C* on the left side of *O* is inconsequential because the orientations *O* and *CO* are equivalent due to the crystal symmetry, so also the patterns for *OC* and *COC* are identical.

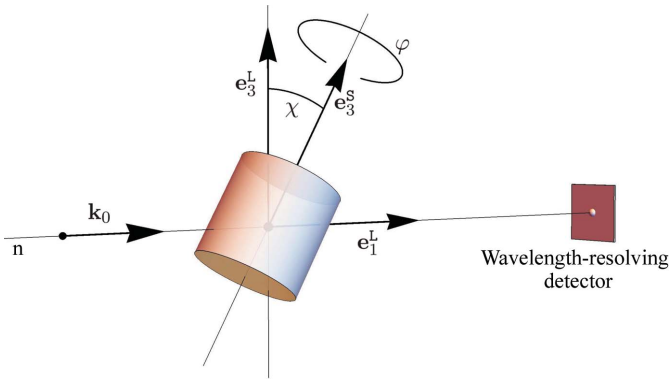

Figure 2
Schematic geometry of the experimental setup with the sample rotation axis inclined to the neutron beam direction.

orientations leading to identical patterns. Since this geometry does not allow for calculating the last component of **d**, the reciprocal-lattice vectors are not fully determinable, which makes the geometry inconvenient for calculating lattice parameters or strain tensors.

3.2. The case with inclined rotation axis

All components of **d** can be obtained when the absolute value of the determinant (7) is sufficiently large. It reaches maximum when $\chi = \arctan\left(1/\sqrt{2}\right) \approx 35.264^\circ$ and the separation between the angles φ_i is the largest possible.

The simplest scheme for computing **d** is to use φ and λ of appropriately selected points on a sinusoid. With χ significantly different from 0 and $\pi/2$, three such points are sufficient, but clearly, a better approach is to use more, say J, points and compute **d** by solving the linear least-squares problem $\min \sum_{j=1}^{J} (\hat{\mathbf{k}}^{\mathrm{S}}(\varphi_j) \cdot \mathbf{d} - \lambda(\varphi_j))^2$. Formally, its solution is

$$\mathbf{d} = \left(K_{\mathrm{S}}^{+}\right)^{T} \boldsymbol{\lambda}, \tag{8}$$

where $\boldsymbol{\lambda} = [\lambda(\varphi_1)\,\lambda(\varphi_2)\,\ldots\,\lambda(\varphi_J)]^T$, $K_{\mathrm{S}} = [\hat{\mathbf{k}}^{\mathrm{S}}(\varphi_1)\,\hat{\mathbf{k}}^{\mathrm{S}}(\varphi_2)\,\ldots\,\hat{\mathbf{k}}^{\mathrm{S}}(\varphi_J)]$ and K_{S}^{+} is the pseudoinverse of K_{S}. In practice, the pseudoinverse is computed using singular value decomposition.

If the axis inclination angle χ is affected by a small non-zero error ε (in radians), then the relative error of the components d_1 and d_2 of **d** is $\Delta_{1,2} \approx \varepsilon \tan\chi$ and the relative error of d_3 is $\Delta_3 \approx \varepsilon \cot\chi$. (Consistent with what was written in the previous section, $\Delta_{1,2}$ and Δ_3 become infinite when $\chi = \pi/2$ and $\chi = 0$, respectively.) Analogous expressions for errors of components of **g** involve $\lambda(\varphi_j)$ and are complicated, but with χ near $\pi/4$, the relative errors of components of **d** are close to ε, and if all components of **d** are modified with the same relative error ε, then the relative error of components of $\mathbf{g} = -2\mathbf{d}/\mathbf{d}^2$ is $\varepsilon/(1+\varepsilon) \approx \varepsilon$. This gives a rough estimate of the sensitivity of the reciprocal-lattice vector determination to the inclination angle χ.

3.3. Detection of sinusoids by image analysis

When intensities of the transmitted neutron beam are recorded for the angles φ_j changed in equal steps and discrete equidistant wavelengths λ_k, one obtains a dataset of intensities numerated by j and k. The set can be seen as a pixelated grayscale image from which the parameters **d** of individual sinusoids are to be extracted. This can be done automatically. The subject of automatic determination of **d** by image-analysis techniques is beyond the scope of this article, but it is worth making the following remarks.

It is noted in Dessieux *et al.* (2023*a*) that if $\chi = 0$, parameters of sinusoids can be determined using the conventional Hough transform. In this case, equation (4) simplifies to $\lambda(\varphi) = d_1 k_1^{\mathrm{S}}(\varphi) + d_2 k_2^{\mathrm{S}}(\varphi) = d_1 \cos\varphi + d_2 \sin\varphi$. With $x_i = x_i(\varphi, \lambda) = k_i^{\mathrm{S}}(\varphi)/\lambda$ $(i = 1, 2)$, this relationship takes the (intercept) form of the equation for a line: $d_1 x_1 + d_2 x_2 = 1$. Thus, if the image in coordinates (φ, λ) is transformed to coordinates (x_1, x_2), the curve described by the parametric equations $x_i(\varphi) = k_i^{\mathrm{S}}(\varphi)/\lambda(\varphi)$ is a line. In other words, sinusoids in the original image become straight lines in the transformed image. Since values of λ are positive, the image space (x_1, x_2) is bounded, so lines in the image can be detected using Hough transform.[3] The question arises about an analogous procedure in the case of $0 < \chi < \pi/2$. With such χ, equation (4) can be written as $d_1 x_1 + d_2 x_2 + d_3 x_3 = 1$, where $x_i = x_i(\varphi, \lambda) = k_i^{\mathrm{S}}(\varphi)/\lambda$ $(i = 1, 2, 3)$. Thus, the curve described by the parametric equations $x_i(\varphi) = k_i^{\mathrm{S}}(\varphi)/\lambda(\varphi)$ in three-dimensional space belongs to a plane. Formally, the problem of determining **d** comes down to detecting planar features in three-dimensional image space, and there are algorithms for that (*e.g.* Sarti & Tubaro, 2002; Bauer & Polthier, 2008; Limberger & Oliveira, 2015). However, with limited wavelength windows and diffraction patterns containing only parts of sinusoids, the planar curves in the three-dimensional image space are short and such detection is unlikely to work in practice.

Parameters of the sinusoids can be determined using other methods. There are numerous dedicated algorithms for detection of sinusoids of fixed period in digital images. Typical sinusoid detection methods rely on Hough transform modified to find sinusoids rather than straight lines (Thapa *et al.*, 1997; Glossop *et al.*, 1999). These searches are exhaustive but computationally expensive. Therefore, alternative approaches avoiding the Hough transformation have also been proposed; see, *e.g.*, Moran *et al.* (2020), Dias *et al.* (2020) and Sattarzadeh *et al.* (2022). Sinusoid detection can be difficult due to intersections and overlapping of the curves. Moreover, only some of the algorithms for detection of sinusoids are applicable to images obtained from transmission spectra because fragments of sinusoids are missing from the images due to the wavelength window.

A simple way to determine **d** is to detect the position of a dip in a spectrum for a selected φ_j, then check the continuity of the sinusoid in the adjacent spectra at $\varphi_{j\pm1}$, and use (8) to get an approximate **d**. Knowing the approximate **d**, spectra at

[3] With Duda–Hart parameters (ρ, θ) of a line and the expression $\rho = x_1 \cos\theta + x_2 \sin\theta$ usually used for performing Hough transform (Duda & Hart, 1972), the first two components of **d** are $d_1 = \cos\theta/\rho$ and $d_2 = \sin\theta/\rho$, and the dependence of the wavelength on the angle φ takes the form $\lambda(\varphi) = \cos(\theta - \varphi)/\rho$.

$\varphi_{j\pm2}$, $\varphi_{j\pm3}$ *etc.* are checked for dips to validate this **d** and improve its accuracy or discard it and try again. With this approach, the limitation of changing the angle φ in equiangular steps can be abandoned. One can use an adaptive selection of φ_j depending on the results obtained in the previous steps. This may reduce the number of sample orientations needed and shorten the overall measurement time.

4. Indexing of data obtained with an inclined rotation axis

4.1. Indexing for orientation determination

By determining **d** and then **g** from a sinusoid on an experimental pattern, one gets a single approximate relationship $O\mathbf{g} \approx \mathbf{h}$ with unknown orientation O and **h** corresponding to one of the plausible reflecting planes. As a reciprocal-lattice vector, **h** is an integer combination of known basis vectors $\mathbf{a}_{\rm C}^i$ given in the Cartesian reference system attached to the crystal, *i.e.*, $\mathbf{h} = \sum_{i=1}^{3} h_i \mathbf{a}_{\rm C}^i$, where $(h_1\ h_2\ h_3) = (hkl)$ are integers. Since there are many, say M, potential reflecting planes, one has the same number of vectors $\mathbf{h}_m$ ($m = 1, 2, \ldots, M$). Given multiple sinusoids, one has multiple, say N, vectors $\mathbf{g}_n$. The goal is to get O and to ascribe some of the vectors $\mathbf{h}_m$ to vectors $\mathbf{g}_n$. One can express the relationship between the sets of vectors $\mathbf{g}_n$ and $\mathbf{h}_m$ as

$$OG \approx HP, \tag{9}$$

where $G = [\mathbf{g}_1\ \mathbf{g}_2 \ldots \mathbf{g}_N]$, $H = [\mathbf{h}_1\ \mathbf{h}_2 \ldots \mathbf{h}_M]$ and P is an unknown $M \times N$ matrix with zero entries everywhere except the values of 1 at entries mn such that $\mathbf{h}_m$ corresponds to $\mathbf{g}_n$. The point is to determine O and P. The matrix O solves the orientation determination problem and P solves the index assignment problem. This formulation is the same as in other cases of indexing for crystal orientation determination; see Morawiec (2020, 2022). Therefore, the problem can be solved automatically using any reasonably general software for crystal orientation determination.

4.2. *Ab initio* indexing

Knowing a number of reciprocal-lattice vectors $\mathbf{g}_n$, one can determine parameters of the crystal lattice. For each vector, one has

$$\mathbf{g}_n \cdot \mathbf{a}_i^{\rm S} \approx h_i^n, \tag{10}$$

where $(h_1^n\ h_2^n\ h_3^n) = (h^n\ k^n\ l^n)$ are unknown integers and $\mathbf{a}_i^{\rm S}$ ($i = 1, 2, 3$) are unknown basis vectors of the direct lattice in the sample reference frame. Solving the above problem (*i.e.*, determining the vectors $\mathbf{a}_i^{\rm S}$ and the indices h_i^n) is the essence of *ab initio* indexing. It can be performed using one of the programs designed for diffraction data; see, *e.g.*, Duisenberg (1992) or Morawiec (2017, 2022). One needs to note that software for *ab initio* indexing usually proposes multiple solutions, and the choice of the ultimate solution is left to the user.

The related problem of the refinement of lattice parameters also relies on equation (10). The task is to determine the direct lattice basis vectors $\mathbf{a}_i^{\rm S}$ from the known vectors $\mathbf{g}_n$ and their indices h_i^n ($n = 1, 2, \ldots, N$). Using the $3 \times N$ matrix $\tilde{H}$ with the integer entries $\tilde{H}_{in} = h_i^n$, equation (10) can be written in the form $G^T[\mathbf{a}_1^{\rm S}\ \mathbf{a}_2^{\rm S}\ \mathbf{a}_3^{\rm S}] \approx \tilde{H}^T$, and one looks for the best matching matrix $[\mathbf{a}_1^{\rm S}\ \mathbf{a}_2^{\rm S}\ \mathbf{a}_3^{\rm S}]$. The least-squares solution to the problem can be written as

$$[\mathbf{a}_1^{\rm S}\ \mathbf{a}_2^{\rm S}\ \mathbf{a}_3^{\rm S}] = (\tilde{H}G^{+})^T.$$

Such refinement is usually the final operation of *ab initio* indexing. Needless to say, the above formula is also the basis for determining elastic strain tensors.

4.3. Compliance check

The proposed strategy of data analysis comes down to the following: Based on the coordinates (φ, λ) of points of a sinusoid, its parameters **d** are calculated using (8), and then the corresponding reciprocal-lattice vector **g** is obtained from (5). This step is repeated for several sinusoids. The thus-obtained set of reciprocal-lattice vectors $\mathbf{g}_n$ ($n = 1, 2, \ldots, N$) allows for the determination of crystal orientation or lattice parameters using existing indexing software. The practical usefulness of the strategy will depend on the accuracy of the $\mathbf{g}_n$ vectors. The lower the accuracy, the more difficult the indexing. While indexing ideal data is straightforward, it is worth confirming that the scheme for determination of the $\mathbf{g}_n$ vectors is consistent with the indexing procedures.

To illustrate the consistency test, data from the window shown in Fig. 3 are used. Wavelengths of eight deepest dips in spectra for $\varphi = 30°$, $60°$ and $90°$ were calculated. Based on equations (6), eight vectors $\mathbf{g}_n$ were obtained. These vectors were input to the orientation determining program *KiKoCh2* (Morawiec, 2020). The resulting orientation was $(\bar{1}\,\bar{2}\,3)[6\,3\,4]$, which is symmetry-equivalent to the original variant of the S orientation. The same set of $\mathbf{g}_n$ vectors was used as input to the program *Ind_X* (Morawiec, 2017) to test *ab initio* indexing. With suitably chosen parameters of *Ind_X*, the program

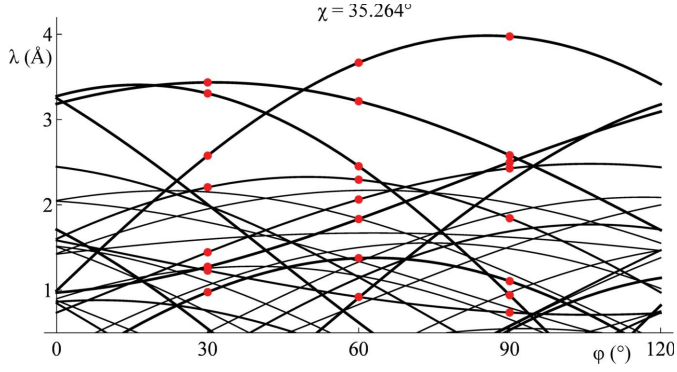

Figure 3
Pattern in the wavelength window 0.5–4.2 Å and φ in the range from 0 to 120°. This is a part of the pattern shown in Fig. 1(*a*). Red discs mark points of the eight sinusoids used for the compliance check.

provided a primitive lattice cell which, after application of *LEPAGE* (Spek, 1988), led to the conventional face-centered-cubic cell with a = 3.613 Å.

Summarizing, in both cases (indexing for orientation determination and *ab initio* indexing), the data used to simulate the pattern were recovered, which means that the compliance tests confirmed the suitability of the proposed strategy.

5. Concluding remarks

Wavelength-resolved neutron imaging can be used for characterization of crystal lattices. Attenuation of the transmitted beam caused by diffraction leads to Bragg dips in transmission spectra at positions corresponding to diffraction reflections. If spectra are collected at different sample orientations, the positions of the dips provide a basis for determination of the crystal orientation and lattice parameters. The simplest way to change the sample orientation is by stepwise rotation about a fixed axis with a spectrum recorded at each step. The resulting pattern of intensities depends on the rotation angle and the wavelength and contains characteristic sinusoids. Each sinusoid represents the dependence of the wavelength on the angle of rotation for reflections from a crystal plane. The sinusoid can be used for determination of coordinates of the reciprocal-lattice vector corresponding to the plane. Crystal orientations and lattice parameters are determined from sets of such vectors.

The usual approach is to rotate the sample about an axis perpendicular to the beam direction. However, it is shown above that the rotation about such an axis is not optimal for determination of the reciprocal-lattice vectors from the sinusoids. A reciprocal-lattice vector can be uniquely determined from coordinates of points of the corresponding sinusoid only if the rotation axis is inclined to the beam direction. It is also shown that having a set of such vectors, one can compute the crystal orientation or lattice parameters using existing indexing software.

The above considerations concern patterns composed of multiple spectra obtained from a single crystal, but the results presented are also relevant for indexing individual spectra, and also for orientation mappings of multigrain samples. Moreover, the considerations are focused on the configuration with a fixed axis of sample rotation, but they can be generalized to indexing of data obtained from spectra collected at arbitrarily set sample orientations.

This article covers only theoretical aspects of determination of lattice geometry from neutron transmission spectra and ignores experimental issues. It should be noted that on the experimental side, the key to accurate reciprocal-lattice vectors is the wavelength resolution. Neutron time-of-flight spectra are characterized by a high density of peaks at short wavelengths (*i.e.*, at the bottom of patterns of sinusoidal curves), and sufficiently high resolution is needed to resolve the peaks and to get their positions.

APPENDIX *A*

Indexing Bragg dips in a single spectrum

A simple approach to indexing Bragg dips in individual spectra is based on the use of a cutoff wavelength equal to double the interplanar spacing of a family of reflecting planes (Santisteban, 2005; Shishido *et al.*, 2023): if a dip is at a wavelength larger than the cutoff wavelength of a family, it must be due to reflection from a stack of planes with larger spacing. This helps in determining the indices of the first dip at the largest wavelengths. The remaining dips are indexed by considering orientations rotated about an axis perpendicular to the stack of planes responsible for the first dip. Forward indexing has also been used for analyzing individual spectra (Sato *et al.*, 2017): the wavelengths of dips were computed for a grid over the domain of transmitted beam directions, and the beam direction was determined by matching the experimental spectrum to these simulated data.

Bragg dips can be indexed by other methods suitable for automation. The most robust ones are based on accumulation of contributions from some primitive configurations. Such methods are used for feature extraction from data (*e.g.* Hough transform) and also in indexing for orientation determination (Ohba *et al.*, 1981; Morawiec, 2022). A simple algorithm of this type (with pairs of Bragg dips voting for beam directions) is sketched below. For this purpose, one needs a formula for computing the beam direction from positions of two Bragg dips and corresponding $\mathbf{h}$ vectors.

A1. Beam direction from positions and indices of two Bragg dips

The direction of the incident beam in the crystal reference frame is $\hat{\mathbf{k}}^{\mathrm{C}} = O\hat{\mathbf{k}}^{\mathrm{S}} = OR_{\varphi}^{T}\hat{\mathbf{k}}_0$, and equation (3) can be written in the form $\mathbf{h}\cdot\hat{\mathbf{k}}^{\mathrm{C}} + \lambda\,\mathbf{h}^2/2 = 0$. Relationships

$$\mathbf{h}_i\cdot\hat{\mathbf{k}}^{\mathrm{C}} + \lambda_i\,\mathbf{h}_i^2/2 = 0, \quad i = 1, 2,$$

between wavelengths λ_1, λ_2 and independent vectors $\mathbf{h}_1$, $\mathbf{h}_2$ plus the normalization condition $\hat{\mathbf{k}}^{\mathrm{C}}\cdot\hat{\mathbf{k}}^{\mathrm{C}} = 1$ constitute a system of three equations for $\hat{\mathbf{k}}^{\mathrm{C}}$. The solution to this system is

$$\hat{\mathbf{k}}^{\mathrm{C}} = \frac{\mathbf{y}\times\mathbf{z} \pm \mathbf{y}\sqrt{4\mathbf{y}^2 - \mathbf{z}^2}}{2\mathbf{y}^2}, \tag{11}$$

where $\mathbf{y} = \mathbf{h}_1\times\mathbf{h}_2$, $\mathbf{z} = \left(\lambda_1\mathbf{h}_1^2\right)\mathbf{h}_2 - \left(\lambda_2\mathbf{h}_2^2\right)\mathbf{h}_1$ and $4\mathbf{y}^2 \geq \mathbf{z}^2$. Thus, if the dips at λ_1 and λ_2 are due to $\mathbf{h}_1$ and $\mathbf{h}_2$, respectively, the beam direction is along one of the vectors given by equation (11). Clearly, if the pairs λ_1, $\mathbf{h}_1$ and λ_2, $\mathbf{h}_2$ are exchanged, one obtains the same vectors $\hat{\mathbf{k}}^{\mathrm{C}}$. If vectors $\mathbf{h}_1$ and $\mathbf{h}_2$ are replaced by $-\mathbf{h}_1$ and $-\mathbf{h}_2$, respectively, then $\mathbf{y}$ remains unchanged and $\mathbf{z}$ changes to $-\mathbf{z}$. Hence, if the pair $\mathbf{h}_1$ and $\mathbf{h}_2$ leads to the pair of vectors $\hat{\mathbf{k}}^{\mathrm{C}}$ given by equation (11), $-\mathbf{h}_1$ and $-\mathbf{h}_2$ lead to the pair of opposite vectors.

A2. Voting for beam direction

Indexing of Bragg dips in a single spectrum based on a known crystal lattice is equivalent to determination of the transmitted beam direction in the crystal coordinate system. The algorithm for determination of the beam direction can be

analogous to one of those used for orientation determination (Morawiec, 2022). One knows the positions of dips λ_k ($k = 1, 2, \ldots, K$). Knowing lattice parameters and families of reflecting planes, one has the reciprocal-lattice vectors $\mathbf{h}_m$ ($m = 1, 2, \ldots, M$). The domain of the beam direction depends on the crystal point symmetry (*e.g.* in the cubic case it is the standard triangle). The domain constitutes the parameter space. In the simplest approach, the space is divided into bins. The first step is to set the counters assigned to the bins to zero. The main computations are based on loops over all pairs of wavelengths $(\lambda_{k_1}, \lambda_{k_2})$, and over all pairs of independent vectors $(\mathbf{h}_{m_1}, \mathbf{h}_{m_2})$. For given $(\lambda_{k_1}, \lambda_{k_2})$ and $(\mathbf{h}_{m_1}, \mathbf{h}_{m_2})$, using equation (11), one obtains a pair of $\hat{\mathbf{k}}^{\mathrm{C}}$ vectors or no solution; in the former case the counters of the bins containing $\hat{\mathbf{k}}^{\mathrm{C}}$ are increased by 1. As a result of these computations, the counters assigned to the bins take on new values. The vector $\hat{\boldsymbol{\kappa}}^{\mathrm{C}}$ corresponding to the bin with the largest counter is the beam direction. In the end, it is worth refining $\hat{\boldsymbol{\kappa}}^{\mathrm{C}}$ by fitting dip positions.

Application of the above scheme to experimental dip positions listed in Table 1 of Santisteban (2005) led to $\hat{\boldsymbol{\kappa}}^{\mathrm{C}} = [0.7407\ \ 0.6717\ \ 0.0142]^T$ [2.9° away from $\langle 1\,1\,0\rangle$ declared in Santisteban (2005)]. The root-mean-square deviation between the experimental and computed positions was 2.4×10^{-4} Å.

A3. Crystal orientation from beam directions

The beam directions obtained by indexing individual spectra can be used for further crystallographic analyses. For instance, they can be a basis for orientation determination: with J ($J \geq 3$) distinct transmission spectra indexed, one has the same number of resulting beam directions $\hat{\boldsymbol{\kappa}}_j^{\mathrm{C}}$ ($j = 1, 2, \ldots, J$), each reduced to the domain used in the indexing procedure. The direction $\hat{\boldsymbol{\kappa}}_j^{\mathrm{C}}$ is equivalent to $S\hat{\boldsymbol{\kappa}}_j^{\mathrm{C}}$, where the matrix S represents a symmetry operation from the crystal point group. For each pair $\hat{\boldsymbol{\kappa}}_j^{\mathrm{C}}$ and $\hat{\mathbf{k}}^{\mathrm{S}}(\varphi_j)$, there exists an operation S_j such that these vectors are related by $S_j\hat{\boldsymbol{\kappa}}_j^{\mathrm{C}} \approx O\hat{\mathbf{k}}^{\mathrm{S}}(\varphi_j)$. First, one needs to determine the operations S_j based on the fact that the vectors $\hat{\mathbf{k}}_j^{\mathrm{C}} = S_j\hat{\boldsymbol{\kappa}}_j^{\mathrm{C}}$ consistent with $\hat{\mathbf{k}}^{\mathrm{S}}(\varphi_j)$ satisfy the relationships $\hat{\mathbf{k}}_{j_1}^{\mathrm{C}} \cdot \hat{\mathbf{k}}_{j_2}^{\mathrm{C}} \approx \hat{\mathbf{k}}^{\mathrm{S}}(\varphi_{j_1}) \cdot \hat{\mathbf{k}}^{\mathrm{S}}(\varphi_{j_2})$ for j_1 and j_2 in $\{1, 2, \ldots, J\}$. Clearly, the result is not unambiguous: if vectors $\hat{\mathbf{k}}_j^{\mathrm{C}}$ satisfy these relations, then the vectors $-\hat{\mathbf{k}}_j^{\mathrm{C}}$ also satisfy them. With $K_{\mathrm{C}} = [\hat{\mathbf{k}}_1^{\mathrm{C}}\ \hat{\mathbf{k}}_2^{\mathrm{C}} \ldots \hat{\mathbf{k}}_J^{\mathrm{C}}]$, K_{S} defined in Section 3.2 and $\hat{\mathbf{k}}_j^{\mathrm{C}} \approx O\hat{\mathbf{k}}^{\mathrm{S}}(\varphi_j)$, one has $K_{\mathrm{C}} \approx OK_{\mathrm{S}}$. Hence, if $0 < \chi < \pi/2$, the crystal orientation is

$$O \approx \mathcal{SO}(K_{\mathrm{C}}K_{\mathrm{S}}^{+}),$$

where $\mathcal{SO}(A)$ denotes the special orthogonal matrix nearest to the matrix A.[4] The choice between $K_{\mathrm{C}} = [\hat{\mathbf{k}}_1^{\mathrm{C}}\ \hat{\mathbf{k}}_2^{\mathrm{C}} \ldots \hat{\mathbf{k}}_J^{\mathrm{C}}]$ and $K_{\mathrm{C}} = -[\hat{\mathbf{k}}_1^{\mathrm{C}}\ \hat{\mathbf{k}}_2^{\mathrm{C}} \ldots \hat{\mathbf{k}}_J^{\mathrm{C}}]$ is resolved by the condition $\det(K_{\mathrm{C}}K_{\mathrm{S}}^{+}) > 0$.

With a slight modification, the above approach can be used to obtain orientations from data collected with the crystal rotation axis perpendicular to the beam direction ($\chi = 0$). The choice of the symmetry operations S_j needed to get $\hat{\mathbf{k}}_j^{\mathrm{C}} = S_j\hat{\boldsymbol{\kappa}}_j^{\mathrm{C}}$ is resolved by comparing the angles between $\hat{\mathbf{k}}_{j_1}^{\mathrm{C}}$ and $\hat{\mathbf{k}}_{j_2}^{\mathrm{C}}$ to $\varphi_{j_1} - \varphi_{j_2}$ [as vectors $\hat{\mathbf{k}}_j^{\mathrm{C}}$ consistent with $\hat{\mathbf{k}}^{\mathrm{S}}(\varphi_j)$ satisfy the relationship $\hat{\mathbf{k}}_{j_1}^{\mathrm{C}} \cdot \hat{\mathbf{k}}_{j_2}^{\mathrm{C}} \approx \cos(\varphi_{j_1} - \varphi_{j_2})$]. Since the third components of the vectors $\hat{\mathbf{k}}^{\mathrm{S}}(\varphi_j)$ are zero, the third column of K_{S}^{+} is zero, and in effect the third column of $K_{\mathrm{C}}K_{\mathrm{S}}^{+}$ is zero, *i.e.*, $K_{\mathrm{C}}K_{\mathrm{S}}^{+}$ has the form $[\mathbf{q}_1\ \mathbf{q}_2\ \mathbf{0}]$. The first two columns of $K_{\mathrm{C}}K_{\mathrm{S}}^{+}$ approximate the first two columns of O. Since the matrix O is special orthogonal, its third column is the vector product of its first and second columns. Thus, the crystal orientation is $O \approx \mathcal{SO}([\mathbf{q}_1\ \mathbf{q}_2\ \mathbf{q}_1 \times \mathbf{q}_2])$. With $K_{\mathrm{C}} = -[\hat{\mathbf{k}}_1^{\mathrm{C}}\ \hat{\mathbf{k}}_2^{\mathrm{C}} \ldots \hat{\mathbf{k}}_J^{\mathrm{C}}]$, one obtains the second possible orientation $\mathcal{SO}([-\mathbf{q}_1\ -\mathbf{q}_2\ \mathbf{q}_1 \times \mathbf{q}_2]) \approx OC$. This is another exposition of the two-way ambiguity in determining orientation when $\chi = 0$.

[4] If the singular value decomposition of A is $A = U\Sigma V^T$, then $\mathcal{SO}(A) = USV^T$ where $S = \mathrm{diag}[+1, +1, \mathrm{sign}(\det(A))]$; see *e.g.* Morawiec (2022).

References

Anderson, I. S., McGreevy, R. L. & Bilheux, H. Z. (2009). Editors. *Neutron Imaging and Applications. A Reference for the Imaging Community.* New York: Springer.

Bauer, U. & Polthier, K. (2008). *Int. Conf. Geom. Modeling Process.* pp. 119–126. Springer.

Bunge, H. J. (1982). *Texture Analysis in Materials Science.* London: Butterworths.

Cereser, A., Strobl, M., Hall, S. A., Steuwer, A., Kiyanagi, R., Tremsin, A. S., Knudsen, E. B., Shinohara, T., Willendrup, P. K., da Silva Fanta, A. B., Iyengar, S., Larsen, P. M., Hanashima, T., Moyoshi, T., Kadletz, P. M., Krooß, P., Niendorf, T., Sales, M., Schmahl, W. W. & Schmidt, S. (2017). *Sci. Rep.* **7**, 9561.

Dessieux, L. L., Stoica, A. D., Frost, M. J. & dos Santos, A. M. (2023*a*). *J. Appl. Cryst.* **56**, 477–490.

Dessieux, L. L., Stoica, A. D., Frost, M. J. & dos Santos, A. M. (2023*b*). *J. Appl. Cryst.* **56**, 491–501.

Dias, L. O., Bom, C. R., Faria, E. L., Valentín, M. B., Correia, M. D., de Albuquerque, M. P., de Albuquerque, M. P. & Coelho, J. M. (2020). *J. Petrol. Sci. Eng.* **191**, 107099.

Duda, R. O. & Hart, P. E. (1972). *Commun. ACM*, **15**, 11–15.

Duisenberg, A. J. M. (1992). *J. Appl. Cryst.* **25**, 92–96.

Frikkee, E. (1975). *Nucl. Instrum. Methods*, **125**, 307–312.

Glossop, K., Lisboa, P. J. G., Russell, P. C., Siddans, A. & Jones, G. R. (1999). *Comput. Vis. Image Underst.* **74**, 96–100.

Halpern, O., Hamermesh, M. & Johnson, M. H. (1941). *Phys. Rev.* **59**, 981–996.

Limberger, F. A. & Oliveira, M. M. (2015). *Pattern Recognit.* **48**, 2043–2053.

Malamud, F. & Santisteban, J. R. (2016). *J. Appl. Cryst.* **49**, 348–365.

Moran, M. B. H., Cuno, J. S., Riveaux, J. A., Vasconcellos, E. C., Biondi, M., Clua, E. W., Correia, M. D. & Conci, A. (2020). *Int. Conf. Systems Signals Image Process. (IWSSIP)*, pp. 255–260.

Morawiec, A. (2004). *Orientations and Rotations. Computations in Crystallographic Textures.* Berlin: Springer.

Morawiec, A. (2017). *J. Appl. Cryst.* **50**, 647–650.

Morawiec, A. (2020). *Acta Cryst.* A**76**, 719–734.

Morawiec, A. (2022). *Indexing of Crystal Diffraction Patterns. From Crystallography Basics to Methods of Automatic Indexing.* Cham: Springer.

Ohba, R., Uehira, I. & Hondoh, T. (1981). *Jpn. J. Appl. Phys.* **20**, 811–816.

Sakurai, Y., Sato, H., Adachi, N., Morooka, S., Todaka, Y. & Kamiyama, T. (2021). *Appl. Sci.* **11**, 5219.

Santisteban, J. R. (2005). *J. Appl. Cryst.* **38**, 934–944.

Santisteban, J. R., Edwards, L., Steuwer, A. & Withers, P. J. (2001). *J. Appl. Cryst.* **34**, 289–297.

Sarti, A. & Tubaro, S. (2002). *Signal Process.* **82**, 1269–1282.
Sato, H., Sasaki, T., Moriya, T., Ishikawa, H., Kamiyama, T. & Furusaka, M. (2018). *Physica B*, **551**, 452–459.
Sato, H., Shiota, Y., Morooka, S., Todaka, Y., Adachi, N., Sadamatsu, S., Oikawa, K., Harada, M., Zhang, S., Su, Y., Kamiyama, T., Ohnuma, M., Furusaka, M., Shinohara, T. & Kiyanagi, Y. (2017). *J. Appl. Cryst.* **50**, 1601–1610.
Sattarzadeh, S., Shalmani, S. M. & Azad, S. (2022). *Proc. IEEE/CVF Conf. Comput. Vision Pattern Recognit.*, pp. 4840–4849.
Shishido, H., Vu, T. D., Aizawa, K., Kojima, K. M., Koyama, T., Oikawa, K., Harada, M., Oku, T., Soyama, K., Miyajima, S., Hidaka, M., Suzuki, S. Y., Tanaka, M. M., Kawamata, S. & Ishida, T. (2023). *J. Appl. Cryst.* **56**, 1108–1113.
Spek, A. L. (1988). *J. Appl. Cryst.* **21**, 578–579.
Strickland, J., Tassenberg, K., Sheppard, G., Nenchev, B., Perry, S., Li, J., Dong, H., Burca, G., Kelleher, J. & Irwin, S. (2020). *Sci. Rep.* **10**, 20751.
Thapa, B. B., Hughett, P. & Karasaki, K. (1997). *Geophysics*, **62**, 129–137.
Thiyagarajan, P., Crawford, R. K. & Mildner, D. F. R. (1998). *J. Appl. Cryst.* **31**, 841–844.
Watanabe, K., Matsumoto, K., Unitani, A., Hitomi, K., Nogami, M. & Kockelmann, W. (2020). *Sens. Mater.* **32**, 1435–1443.
Watanabe, K., Sugai, Y., Hasegawa, S., Hitomi, K., Nogami, M., Shinohara, T., Su, Y., Parker, J. D. & Kockelmann, W. (2024). *Sens. Mater.* **36**, 149–154.
Woracek, R., Santisteban, J., Fedrigo, A. & Strobl, M. (2018). *Nucl. Instrum. Methods Phys. Res. A*, **878**, 141–158.